Theor. Comput. Fluid Dyn. (2017) 31:607–621
DOI 10.1007/s00162-017-0426-0

ORIGINAL ARTICLE

Renan de S. Teixeira · Leonardo S. de B. Alves

Minimal gain marching schemes: searching for unstable steady-states with unsteady solvers

Received: 15 February 2016 / Accepted: 22 February 2017 / Published online: 7 March 2017

Abstract Reference solutions are important in several applications. They are used as base states in linear stability analyses as well as initial conditions and reference states for sponge zones in numerical simulations, just to name a few examples. Their accuracy is also paramount in both fields, leading to more reliable analyses and efficient simulations, respectively. Hence, steady-states usually make the best reference solutions. Unfortunately, standard marching schemes utilized for accurate unsteady simulations almost never reach steady-states of unstable flows. Steady governing equations could be solved instead, by employing Newton-type methods often coupled with continuation techniques. However, such iterative approaches do require large computational resources and very good initial guesses to converge. These difficulties motivated the development of a technique known as selective frequency damping (SFD) (Åkervik et al. in Phys Fluids 18(6):068102, 2006). It adds a source term to the unsteady governing equations that filters out the unstable frequencies, allowing a steady-state to be reached. This approach does not require a good initial condition and works well for self-excited flows, where a single nonzero excitation frequency is selected by either absolute or global instability mechanisms. On the other hand, it seems unable to damp stationary disturbances. Furthermore, flows with a broad unstable frequency spectrum might require the use of multiple filters, which delays convergence significantly. Both scenarios appear in convectively, absolutely or globally unstable flows. An alternative approach is proposed in the present paper. It modifies the coefficients of a marching scheme in such a way that makes the absolute value of its linear gain smaller than one within the required unstable frequency spectra, allowing the respective disturbance amplitudes to decay given enough time. These ideas are applied here to implicit multi-step schemes. A few chosen test cases shows that they enable convergence toward solutions that are unstable to stationary and oscillatory disturbances, with either a single or multiple frequency content. Finally, comparisons with SFD are also performed, showing significant reduction in computer cost for complex flows by using the implicit multi-step MGM schemes.

Keywords Linear stability analysis · Numerical analysis · Gain reduction · Unstable spectra · Stationary and oscillatory disturbances · Truncation error

Communicated by Vassilios Theofilis.

Renan de S. Teixeira
Programa de Pós-Graduação em Engenharia de Defesa, Instituto Militar de Engenharia, Rio de Janeiro, RJ 22290-270, Brazil
E-mail: rsteixeira-pronametro@inmetro.gov.br

Leonardo S. de B. Alves (✉)
Laboratório de Mecânica Teórica e Aplicada, Departamento de Engenharia Mecânica, Universidade Federal Fluminense, Niterói, RJ 24210-240, Brazil
E-mail: leonardo.alves@mec.uff.br

1 Introduction

Reference solutions are necessary in several fluid dynamic research areas. One such area is linear stability analysis, where they represent the base state whose linear stability is being investigated. Earlier investigations of planar mixing-layers and free jets used analytical functions, that fit well enough experimental data, as reference solutions [30]. In complex flows however, these approximations may lead to incorrect predictions. The transverse jet linear stability analysis of a base state generated by a similarity solution of the boundary-layer equations shows a decrease in the range of unstable frequencies as the cross flow velocity increases [23]. However, a similar analysis using an analytical fit of available data as its base state shows the opposite trend [4]. The former base state is closer to a solution of the Navier-Stokes equations than the latter one, which is the most likely reason why the former trend is the one that agrees with experimental data [29]. Since they are not solutions of the steady-state governing equations, approximate base states introduce a forcing term in the disturbance governing equations that affects their dynamics. Such a forcing can be subtracted from the original governing equations, making the approximate base state a solution of the resulting modified equations. This procedure is akin to the method of manufactured solutions for code verification [36]. It was used to evaluate the behavior of small disturbances superposed to an approximate base state in the study of laminar separation bubbles [20]. On the other hand, this particular base state was a time-averaged mean solution of the original unsteady governing equations. It is well known that mean solutions can lead to qualitatively incorrect predictions when compared to steady-states [5]. Given the latest advances in linear stability analysis [12,34,38], a procedure that generates steady-states of unstable flows would be very useful.

Another area where reference solutions are necessary is computational fluid dynamics. Initial conditions represent one example. For instance, approximate analytical fits of experimental data as well as similar solutions of the boundary-layer equations introduce unwanted oscillations when used as initial conditions in the unsteady numerical simulation of absolutely unstable mixing-layers [25]. Their amplitude is smaller in the latter case, but their frequency content is richer as well. This problem also manifests itself in the calculation of temporal growth rates, which can have relative errors as high as 18% [19]. Inaccurate initial conditions in simulations of flows around two-dimensional bodies create large numerical disturbances at early times [8,39]. Hence, large simulation times are required for these numerical waves to leave the simulated domain before accurate flow statistics can be extracted. Boundary conditions represent another example within this area [14]. Reference solutions are useful for absorbing layers [9] or sponge zones [10], but their effectiveness depends on their accuracy. This is specially relevant in aeroacoustics [15] and receptivity [33] studies, where physical disturbances of interest are much smaller in magnitude than vorticity waves. In the simulation of acoustic fields over airfoils [13], these problems were minimized with the use of steady-states as reference solutions for both initial conditions and sponge zones. A similar procedure was adopted to minimize numerical errors in receptivity studies of compressible mixing-layers [7]. Hence, a procedure capable of generating steady-states for unstable flows would be quite useful in computational fluid dynamics.

Today, there are only two major ways of satisfying this demand for unstable steady-states. The traditional approach uses Newton-type methods to solve the steady governing equations. A vast literature exists on this subject, but its review is beyond the scope of this paper. Nevertheless, modern variations seem to rely on Jacobian free Newton–Krylov methods [24]. Their quadratic or at least super-linear convergence makes them interesting choices, but a few disadvantages exist. For instance, convergence is only guaranteed when a good enough initial guess is provided. Continuation techniques are often employed to overcome this difficulty, but they can only find steady-states connected by continuity [11]. This can be problematic when multiple and disconnected steady-states exit for the same parametric conditions due to complex bifurcation patterns. Finally, initial value problems are much easier to solve than their boundary value counterparts, which means most existing codes solve unsteady governing equations. Hence, the use of Newton-type methods often requires the construction of a new code to solve the steady governing equations. These difficulties led to the development of an alternative method known as selective frequency damping or SFD [1]. It introduces a source term in the unsteady governing equations that forces the time marching scheme to converge toward a reference solution, which is a filtered version of the unsteady solution being marched in time. Since this source term disappears at steady-state, the reference solution becomes the steady-state in this limit. SFD is simple to implement in an existing unsteady code and requires the adjustment of only two additional parameters. These advantages led to its use in several problems, such as cavity flows [2], wakes around spheres [31], jets in cross flows [5] and boundary-layers over roughnesses [27]. Nevertheless, efficiency is highly dependent on these two additional parameters, which is the reason why recent studies have focussed on their optimization [16,22]. Despite its advantages, SFD does have significant drawbacks [21]. For example, it seems unable to converge toward a

steady-state when the governing equations are unstable to stationary disturbances. Furthermore, SFD was originally designed to filter flows that are self-excited by a single frequency [2]. Its application to any flow subject to oscillatory instabilities by multiple dominant frequencies then likely requires the use of multiple filters. This will increase the number of parameters requiring optimization as well as the overall computer cost, making the use of SFD impractical when the flow is unstable to a broad frequency spectrum. Hence, one must continue the search for an alternative to Newton-type methods, since it should be easily applicable to unsteady codes and have little sensitivity to initial conditions, and to SFD as well, since this alternative should also be capable of generating steady-states for any flow independent of its underlaying instability mechanism.

The present paper proposes a new methodology that satisfies these criteria. It is based on classical linear numerical stability concepts in computational fluid dynamics [28]. On a linear basis, a marching scheme is assumed numerically stable if its gain is smaller than one, for a given time step, when the governing equation is physically stable. On the other hand, some special schemes are still numerically stable even when the governing equation they are integrating is physically unstable. The implicit Euler scheme is one such method. For this reason, it has been used in the past to march unstable flows toward steady-states [13,32]. This motivated the recent use of dual-time-stepping as a simple way to switch the marching scheme of arbitrary codes to an implicit Euler scheme [37]. However, there are many instances in which this scheme cannot reach a steady-state. In the next section, the reasons for this behavior are investigated. They motivated the proposal of this new methodology, which is used for the construction of an implicit multi-step scheme with an enhanced ability to generate steady-states. Its performance is then evaluated in Sec. 3 for several test cases representing different instability mechanisms. Finally, main conclusions and next steps forward are presented in Sec. 4.

2 Numerical methodologies

2.1 Modal linear numerical stability

Consider a dynamical system in the form of the homogeneous initial value problem $\mathrm{d}u/\mathrm{d}t = f(u)$. The Taylor series expansion of $f(u)$ around its steady-state u_s yields $f(u) \simeq \lambda\, u_d + O(u_d^2)$, where $\lambda = (\partial f/\partial u)_{u=u_s}$ is an eigenvalue, $u_d(t) = u(t) - u_s$ is a deviation from steady-state and $f(u_s) = 0$. Hence, the linear stability of this system is governed by $\mathrm{d}u_d/\mathrm{d}t = \lambda\, u_d(t)$. Since its solution is $u_d(t) \simeq u_d(0)\ \exp[\,\lambda\, t\,]$, the dynamical system is linearly stable when $\lambda < 0$. Otherwise, the dynamical system is linearly unstable when $\lambda > 0$. This is relevant whenever $u_d(0)$ is a small deviation from u_s. Physical stability is the term used here when referring to the stability of the dynamical system.

Applying an arbitrary multi-step scheme to march this dynamical system in time leads to $u^{n+1} = u^n + \Delta t\ \Delta(u)$, where $n+1$ and n are the unknown and known time step indexes, respectively, Δt is the time step and $\Delta(u)$ represents the temporal discretization employed. According to Lax's equivalence theorem, a discrete scheme, applied to a linear and well-posed initial value problem, converges as long as it is consistent and stable [26]. Convergence in this context means that the discrete solution approaches the continuous one when $\Delta t \to 0$ for a fixed time t. However, the word convergence has a different meaning in the present paper. It implies that a steady-state is achieved when $t \to \infty$ for a fixed Δt. Nonetheless, equivalence considerations are similar and still require consistency as well as stability. A scheme is consistent when the continuous governing equation can be recovered from its discrete counterpart in the limit $\Delta t \to 0$. On the other hand, a scheme is linearly stable when the absolute value of the gain $G = u_d^{n+1}/u_d^n = \exp[\lambda \Delta t]$ is $|G| < 1$ within a certain finite or infinite $\lambda \Delta t$ range, where $u_d^n = u_d(t_n)$ and $t_{n+1} = t_n + \Delta t$. Otherwise, the numerical scheme is linearly unstable when $|G| > 1$. Numerical stability is the term used here when referring to the stability of the marching scheme.

Figure 1 shows $|G|$, on the left plot, and the total number of iterations N required for convergence to $u_d(t) = 10^{-16}$ starting from $u_d(0) = 1$, on the right plot, both as functions of $\lambda \Delta t$ for the explicit Euler (EE), implicit Euler (IE) and second-order Adams-Bashforth (AB2) schemes. All three schemes are consistent. Numerical stability is traditionally evaluated under physically stable conditions, i.e. for $\lambda < 0$. Within this spectral region, EE and AB2 are conditionally stable, since $|G| < 1$ for $-2 < \lambda \Delta t < 0$ and $-1 < \lambda \Delta t < 0$, respectively. In other words, the stability of these schemes is conditioned to the use of finite time steps. On the other hand, IE is A-stable, since $|G| < 1$ for $\lambda \Delta t < 0$. Its stability is actually stronger, since this scheme is L-stable. This means $|G| \to 0$ as $\lambda \Delta t \to -\infty$, whereas A-stability only requires $|G| < 1$ in the same limit. All three schemes converge with a finite N within their respective stability bounds. The dashed line in the right plot of this figure is drawn at $N = 5000$. This number was imposed as an upper bound for N since all

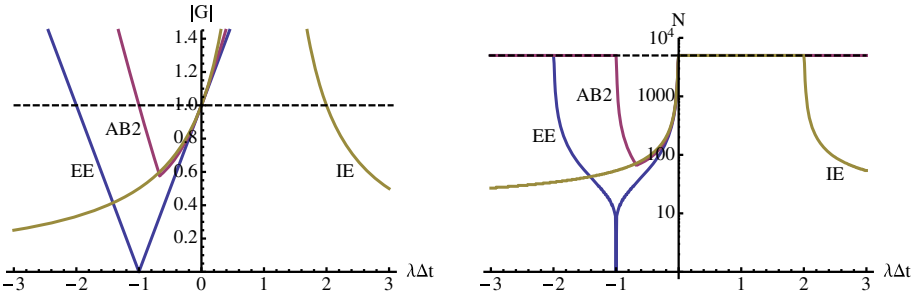

Fig. 1 Absolute value of the gain (*left*) and total number of iterations for convergence (*right*) as functions of the dimensionless time step for EE, IE and AB2 schemes. *Dashed lines* indicate an approximate threshold for instability

simulations diverged if they passed this threshold. Nevertheless, convergence is achieved when Δt is chosen small enough so $\lambda\Delta t$ falls within the stability bounds. Furthermore, N is proportional to $|G|$, where $N \to 1$ when $|G| \to 0$. This leads to an often misunderstood concept. Even though physical intuition might indicate that optimal convergence toward steady-state is achieved by imposing the largest possible time step, a linear numerical stability analysis reveals that optimal convergence is in fact achieved at the time step that yields the smallest absolute value of the gain. Physical intuition is only correct for L-stable schemes, where $|G| \to 0$ as $\Delta t \to \infty$. These well known results, based on a linear stability analysis, show that numerically stable schemes can be used to march physically stable problems to steady-state. Furthermore, the efficiency of this process depends on how small is the gain.

However, as pointed out in the introduction, steady-states of physically unstable problems are even more valuable. In this context, it is paramount to understand numerical stability when $\lambda > 0$ as well. Both explicit schemes in Fig. 1 are numerically unstable within this spectral region. On the other hand, the IE scheme is numerically stable for $\lambda\Delta t > 2$, even though the problem is physically unstable when $\lambda > 0$. It is in this sense doubly L-stable, since $|G| \to 0$ as $\lambda\Delta t \to \pm\infty$. This is the reason why IE is a marching scheme of choice in the literature for the generation of steady-states [13,32,37]. Nonetheless, this scheme achieves convergence for physically unstable problems when Δt is chosen large enough ($\Delta t > 2/\lambda$) so $\lambda\Delta t$ falls within its numerical stability bounds. On the other hand, nonlinearity reduces the maximum allowed time step in most problems. In these cases, one might not be able to make Δt large enough to remove the physically unstable eigenvalue λ from the (linearly) numerically unstable region $0 < \lambda\Delta t < 2$.

2.2 Minimal gain marching (MGM) schemes

Since in most cases the eigenvalue λ is fixed by the physical problem and the time step Δt maximum value is limited by nonlinearities, the only alternative left from a linear stability perspective is to modify the scheme itself in order to reduce its unstable region. Doing so, however, is not straightforward, since a few constraints still must be satisfied. A nonlinear counterpart to Lax's equivalence theorem does not exist, so it is important to guarantee consistency and stability on a linear basis. In order to impose consistency, a truncation error analysis is necessary. Considering the same homogeneous initial value problem from the previous subsection

$$\frac{\mathrm{d}u}{\mathrm{d}t} = f(u), \tag{1}$$

one can march it in time with the general implicit multi-step scheme

$$\frac{a_{+1}\,u^{n+1} + a_0\,u^n + a_{-1}\,u^{n-1}}{\Delta t} = b_{+1}\,f^{n+1} + b_0\,f^n + b_{-1}\,f^{n-1}, \tag{2}$$

where the notation $f^n = f(u^n)$ was employed. Using Taylor series expansions, this discrete equation can be re-written as

$$(a_{+1} - a_{-1})\,\frac{\mathrm{d}u}{\mathrm{d}t} = (b_{+1} + b_0 + b_{-1})\,f(u) + \text{T.E.}, \tag{3}$$

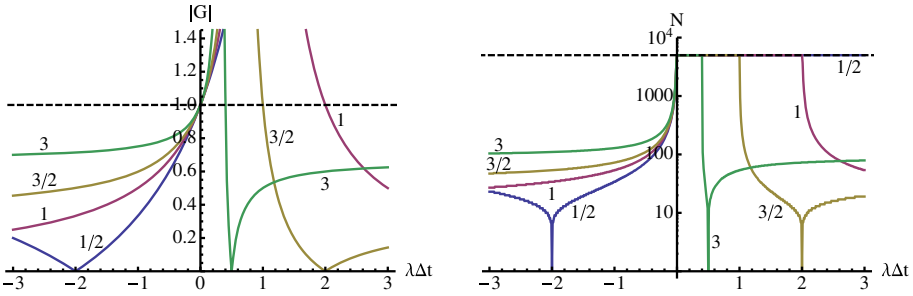

Fig. 2 Same as Fig. 1 but for Eq. (8) with $\theta_1 = 1$ and $\theta_2 = 1/2$, 1, 3/2 and 3

with its truncation error defined as

$$-\text{ T.E.} = \Delta t^{-1}\left(a_{+1} + a_0 + a_{-1}\right) u^n + \Delta t \left\{ \frac{1}{2}\left(a_{+1} + a_{-1}\right) \left.\frac{\mathrm{d}^2 u}{\mathrm{d}t^2}\right|^n - \left(b_{+1} - b_{-1}\right) \left.\frac{\mathrm{d}f}{\mathrm{d}t}\right|^n \right\} + O\left(\Delta t^2\right), \tag{4}$$

which means consistency can be guaranteed by imposing

$$a_{+1} + a_0 + a_{-1} = 0, \tag{5}$$

otherwise $f(u_s) = 0$ is only possible for trivial steady-states $u_s = 0$, and

$$a_{+1} - a_{-1} = b_{+1} + b_0 + b_{-1}, \tag{6}$$

otherwise Eq. (3) would result in a time rescaled version of Eq. (1) in the limit $\Delta t \to 0$. Since temporal accuracy is not necessary to reach steady-state, there is no need for modified schemes with accuracy-orders greater than one. This means no additional constraints are required from a T.E. standpoint.

The final step to satisfy Lax's equivalence theorem is to demonstrate that regions of linear numerical stability exist for Eq. (2). Using the same classical analysis discussed in the previous subsection leads to

$$\left(a_{+1} - \lambda\Delta t\, b_{+1}\right) G^2 + \left(a_0 - \lambda\Delta t\, b_0\right) G + \left(a_{-1} - \lambda\Delta t\, b_{-1}\right) = 0, \tag{7}$$

where the EE scheme has $b_{+1} = 0$, $b_0 = 1$ and $b_{-1} = 0$, the AB2 scheme has $b_{+1} = 0$, $b_0 = 3/2$ and $b_{-1} = -1/2$, and the IE scheme has $b_{+1} = 1$, $b_0 = 0$ and $b_{-1} = 0$, in addition to $a_{+1} = 1$, $a_0 = -1$ and $a_{-1} = 0$ for all three schemes. Their respective gains from Eq. (7) were used to generate the left plot in Fig. 1. If additional steps were added to Eq. (2), say at $n-2$, $n-3$ and so on, Eq. (7) would become an ever higher-order polynomial equation for G. As this polynomial order increases, so does the number of solutions of the resulting equation, all of which must satisfy $|G| < 1$ at some $\lambda\Delta t$ region for stability. Hence, it becomes increasingly harder to find multi-step schemes with large stability regions as their number of coefficients increases. Indirect confirmation comes from the fact that there are no A-stable multi-step schemes with accuracy-order higher than two [17]. Since implicit backwards difference formulas (BDFs) with first (IE) and second (BDF2) accuracy-orders are the best known L-stable multi-step schemes, $b_{-1} = 0$ is imposed here as well. The resulting two parameter family of multi-step schemes is re-written as

$$\theta_1 \frac{u^{n+1} - u^n}{\Delta t} + \left(1 - \theta_1\right) \frac{u^{n+1} - u^{n-1}}{2\,\Delta t} = \theta_2\, f^{n+1} + \left(1 - \theta_2\right) f^n, \tag{8}$$

in order to highlight the discrete temporal derivative as a weighted average between dissipative and non-dissipative approximations. Setting $a_0 = -\theta_1$, $a_{\pm 1} = (\theta_1 \pm 1)/2$, $b_0 = 1 - \theta_2$ and $b_{+1} = \theta_2$ in Eq. (7) leads to its gain. Their linear stability properties are illustrated here for the particular case where $\theta_1 = 1$, since this leads the well-known generalized Crank–Nicolson scheme.

It is used in the literature with either $\theta_2 = 1$ or $1/2$, which are the IE and second-order Crank–Nicolson (CN2) schemes, respectively. Figure 2 shows the same results presented in Fig. 1, but for $\theta_2 = 1/2$, 1, 3/2 and 3. As is already known, the CN2 scheme is A-stable for $\lambda\Delta t < 0$ but unstable otherwise, with $|G| \to 1$ as $\Delta t \to \infty$. When θ_2 is increased to 1, Eq. (8) reverts back to IE, which was discussed and shown Fig. 1. The

important behavior for the purpose of steady-state generation with marching schemes appears when setting $\theta_2 > 1$, a range never reported before as far as the authors are aware. Within this range, Eq. (8) remains A-stable for $\lambda < 0$. Furthermore, its numerically unstable region is $0 < \lambda \Delta t < 2/(2\,\theta_2 - 1)$ for $\lambda > 0$, which means this region decreases in size as θ_2 increases beyond 1/2. As Fig. 2 shows, the original IE scheme unstable region decreases in half when $\theta_2 = 3/2$ and by four times when $\theta_2 = 3$. Although it continues to decrease in size as θ_2 increases, $|G| \to (\theta_2 - 1)/\theta_2$ as $\Delta t \to \infty$. In other words, this asymptotic gain goes to $|G| \to 1$ from below as $\theta_2 \to \infty$. Hence, one can expect stabilization for small but positive $\lambda \Delta t$ but worse convergence for high Δt, which is observed on the right plot of Fig. 2 for positive and negative values of λ. Nevertheless, numerical stabilization of a physically unstable problem can be achieved by increasing θ_2 beyond 1.

In summary, MGM schemes can be derived by following a straightforward methodology. Its goal is to construct marching schemes that are numerically stable on a linear basis when integrating physically unstable flows toward steady-state. The convergence of such schemes is optimal, also on a linear basis, when the chosen Δt yields the smallest possible $|G|$. Since nonlinearities restrict the maximum allowed Δt of any scheme, this derivation should pursue schemes with the smallest possible $|G|$ at the smallest possible Δt. In order to do so, a modal and linear numerical stability analysis should guide the selection of the free coefficients. In the present case, Eq. (7) guides the selection of θ_1, θ_2 and Δt in Eq. (8). For this particular MGM scheme, the guidelines are:

1. Always start the search for steady-states with the implicit Euler ($\theta_1 = \theta_2 = 1$) scheme using the largest possible Δt due to its L-stability.
2. If convergence is not achieved, increase θ_2 and/or decrease θ_1. This process should be gradual, since it removes L-stability, increasing the asymptotic values of $|G|$ away from 0, likely deteriorating convergence rates. It should, however, eventually allow convergence as Δt is decreased.

2.3 Over/under relaxed newton method

An analysis of the asymptotic behavior provides an interesting view about the nature of the control parameter θ_2 in Eq. (8). It is well known that the IE scheme reverts back to a Newton method as $\Delta t \to \infty$ [28]. This method has quadratic convergence and can be used to search for the roots of $f(u) = 0$, which are the steady-states $u = u_s$ of Eq. (1). Evaluating Eq. (8) at the same asymptotic limit and Taylor series expanding $f(u^{n+1})$ up to $O(\Delta u)$ yields

$$\Delta u = u^{n+1} - u^n = -\frac{1}{\theta_2} \frac{f(u^n)}{(\partial f/\partial u)^n}, \tag{9}$$

which is analogous to applying relaxation $u^{n+1} = \omega\, u^{n+1} + (1 - \omega)\, u^n$ to the Newton method, but with a relaxation parameter $\omega = 1/\theta_2$. Hence, imposing $\theta_2 > 1$ is equivalent to under-relaxing ($\omega < 1$) whereas imposing $\theta_2 < 1$ is equivalent to over-relaxing ($\omega > 1$) the marching scheme (Newton method). Within the context of iterative root finding methods, the former often enables convergence of an otherwise diverging Newton method, whereas the latter is used to accelerate convergence of an already converging Newton method. In the context of MGM schemes, under-relaxation stabilizes an otherwise numerically unstable scheme applied to an unstable physical problem. In other words, it makes a diverging scheme convergent. Although this is the main goal of the present paper, the relaxation analogy points to another use for MGM schemes. Over-relaxation should further stabilize an already numerically stable scheme applied to a stable physical problem. In other words, it accelerates convergence of an already converging scheme. This is certainly true for linear problems. As shown in Fig. 2, the gain is reduced when θ_2 decreases from 1 to 1/2 for small negative $\lambda\, \Delta t$ values, which reduces the number of time steps required for convergence. Although this is likely true as well for weakly nonlinear problems, strongly nonlinear problems require further studies. They are, however, beyond the scope of this paper, which focuses on the generation of unstable instead of stable steady-states. The former receives a higher priority because the latter can already be obtained with standard schemes.

2.4 Selective frequency damping

In order to make the paper more self contained, a brief description of SFD is provided [1]. It introduces a source term in Eq. (1), namely

$$\frac{\mathrm{d}u}{\mathrm{d}t} = f(u) - \chi\,(u - \bar{u}), \tag{10}$$

where χ is the stabilization amplitude required to damp the most unstable eigenvalue and $\bar{u}$ is a low-pass temporally filtered variable. When this filter is an exponential kernel, $\bar{u}$ can be obtained in an efficient manner from

$$\frac{\mathrm{d}\bar{u}}{\mathrm{d}t} = \frac{u - \bar{u}}{\Delta}, \tag{11}$$

where Δ is inversely proportional to the cut-off frequency. Although SFD alters the original transient evolution of Eq. (1), $\bar{u} = u_s$ at steady-state and the forcing term in Eq. (10) disappears in this limit. This means Eqs. (1) and (10) yield the same otherwise unstable steady-state. Coupling between Eqs. (1) and (10) was implemented in an explicit manner for all test cases, since the more cumbersome implicit implementation showed negligible improvements.

3 Results and discussion

A few test cases are simulated to evaluate the ability of minimal gain marching (MGM) schemes developed here to reach a steady-state. Several types of flow instability are considered. Whenever possible, the performances of MGM and selective frequency damping (SFD) are compared. The only exceptions are the particular cases where SFD was not able to damp a certain flow instability. It should be noted that comparisons with the over/under relaxed Newton method were not possible when using as initial guesses the same initial conditions employed for MGM and SFD. When doing so, convergence was not achieved. The only exception was the Lorenz equation test case discussed next. Hence, this method is no longer mentioned from this point on.

3.1 Lorenz equations

The first test case used here solves the Lorenz equations [35]

$$\frac{\mathrm{d}x}{\mathrm{d}t} = \sigma\,(y - x), \quad \frac{\mathrm{d}y}{\mathrm{d}t} = x\,(\rho - z) - y \quad \text{and} \quad \frac{\mathrm{d}z}{\mathrm{d}t} = x\,y - \beta\,z, \tag{12}$$

with $\sigma = 10$, $r = 40$ and $b = 8/3$. Figure 3, left plot, shows $x(t)$ obtained using CN2 with a Δt small enough to render $x(t)$ grid independent within $0 < t < 25$ starting from the initial conditions $x(0) = y(0) = z(0) = 1/10$. Thick lines show what happens to this temporal evolution when MGM is turned on at different times. MGM is run at locally optimal conditions $\theta_1 = 1$, $\theta_2 = 2$ and $\Delta t = 0.06$ from Fig. 3, right plot. This figure presents the asymptotic disturbance growth rate λ for different θ_1, θ_2 and Δt. Solid points indicate the smallest Δt capable of reaching $|(x^{n+1} - x^n)/(x^2 - x^1)| = 10^{-8}$. Steady-states are still reached for smaller Δt, but

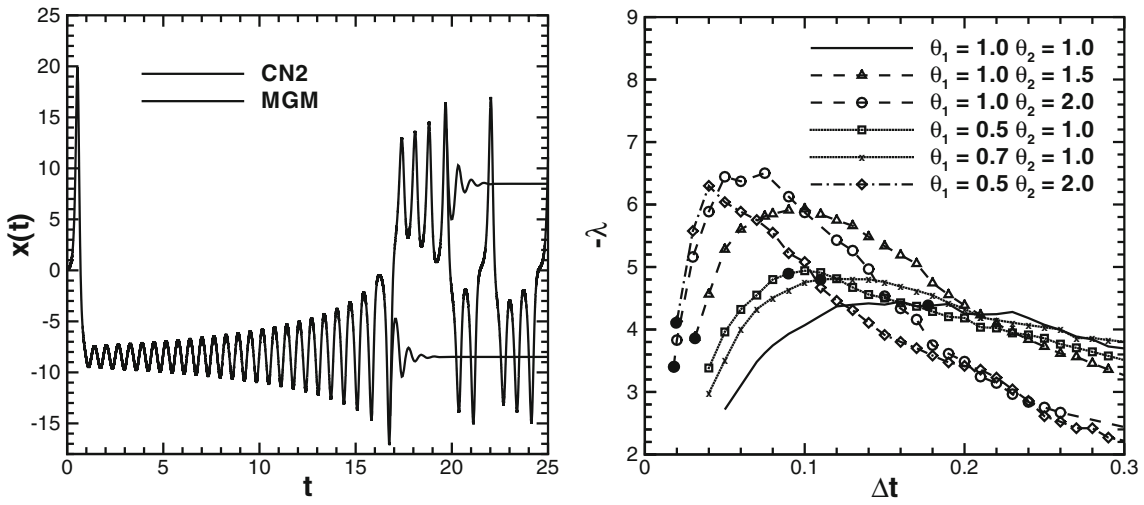

Fig. 3 Lorenz variable unsteadiness (*left*) and MGM disturbance growth rate (*right*)

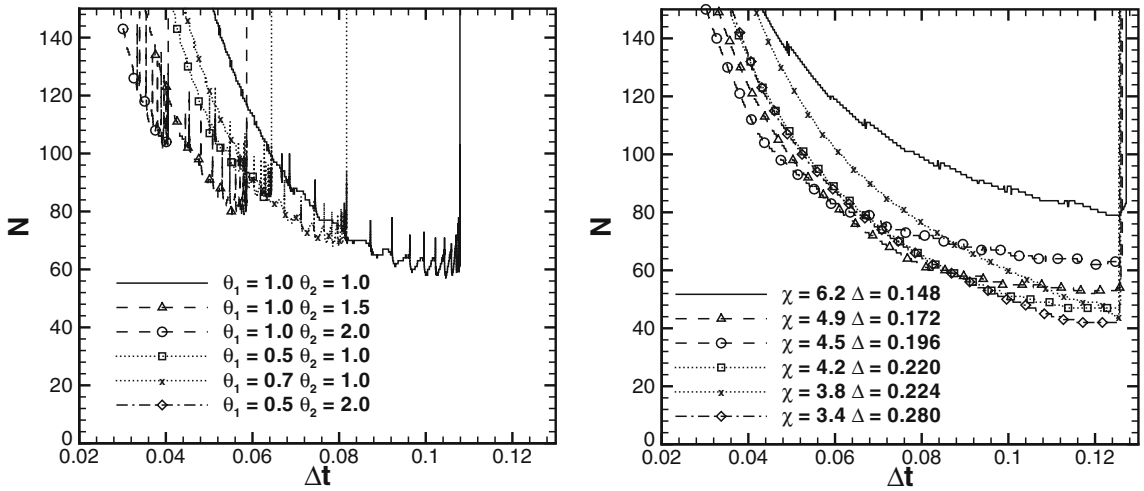

Fig. 4 Number of iterations for convergence with MGM (*left*) and SFD (*right*)

they have lower accuracy. Nevertheless, imposing $\theta_2 > 1$ and/or $\theta_1 < 1$ enables the use of a lower Δt, as predicted by the guidelines based on linear stability at the end of Sect. 2.2.

Figure 4 shows the number of iterations required for convergence toward the same tolerance for MGM (left plot) and SFD (right plot) under different parametric conditions near their respective optimum. All optimum points were estimated by a brute force variation of all respective control parameters. Since SFD is simulated with CN2, cpu time per iteration is very similar between it and MGM simulated with Eq. (8), allowing comparisons between iteration counts instead. These same procedures were employed in all test cases. This figure shows that IE ($\theta_1 = \theta_2 = 1$) is still the best choice when Δt can be made large enough to place all physically unstable eigenvalues outside of its numerically unstable region, since allowing $\theta_1 \neq 1$ and/or $\theta_2 \neq 1$ increases the linear asymptotic gain. Vertical lines on both plots indicate an inability to converge toward the required tolerance when further increasing Δt, analogous to the solid points on the right plot of Fig. 3. MGM optimal points are different between Figs. 3 (right) and 4 (left), but this is due to strong variations in λ during initial transients. Nevertheless, Fig. 4 shows that an optimal IE requires 50% more iterations than optimal SFD to reach the same tolerance. This particular test case, however, is an ideal one for SFD because all steady-states, such as the ones shown in Fig. 3 (left), are unstable to the same frequency. Furthermore, the MGM stabilization was not necessary, since nonlinearities were not strong enough to significantly reduce the maximum time step of the IE scheme. For these reasons, more complex test cases are studied and discussed in the next subsections.

3.2 Modified Burger's equation

A 1D transient and viscous Burger's type equation is considered next [6],

$$\frac{\partial u}{\partial t} + u\,\frac{\partial u}{\partial x} = \frac{1}{Re}\,\frac{\partial^2 u}{\partial x^2} + R\,(u - u_s), \tag{13}$$

where R is the source term control parameter, Re the Reynolds number and u_s represents the steady-state. It becomes convectively unstable at $R = 0$ and transitions to absolutely unstable at $R = Re/4$, where $Re = 32$ is used here. Both onsets of instability are due to stationary and spatially uniform disturbances. Figure 5 shows velocity disturbances at $R = 5$ (left) and $R = 87$ (right), where typical convective and absolute unstable behavior is observed. Simulations employed periodic boundary conditions with a buffer zone near the outflow boundary to enforce the inflow boundary condition $u = u_s = 1$. The flow was disturbed by a Gaussian source term, marked by thin dashed lines in this figure. Discrete approximations used were CN2 in time, fifth-order biased upwind scheme for the advective term and fourth-order central scheme for the diffusive term. Temporal and spatial numerical orders were verified, and results are grid independent and agree well with linear stability data.

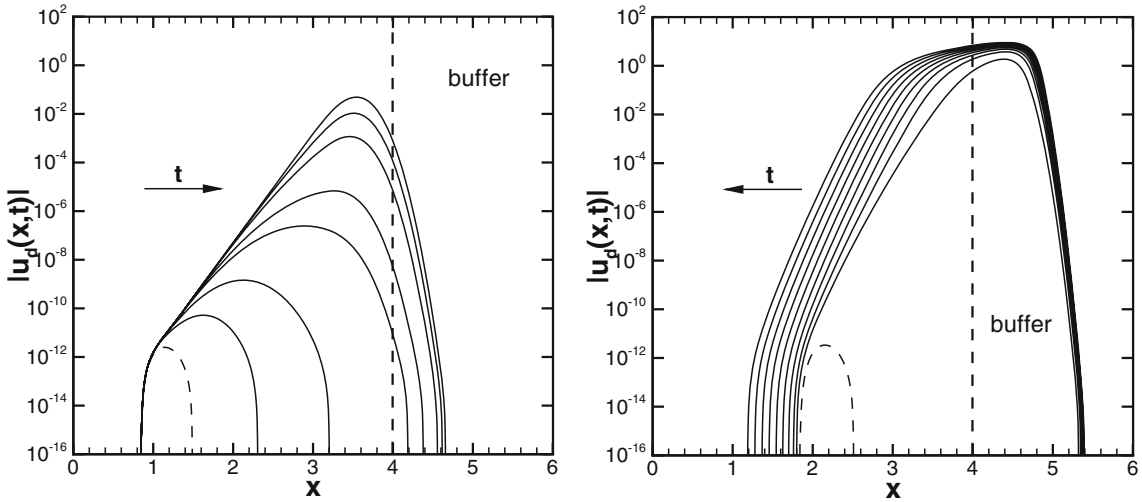

Fig. 5 Modified Burger's equation simulation at $R = 5$ (*left*) and $R = 87$ (*right*)

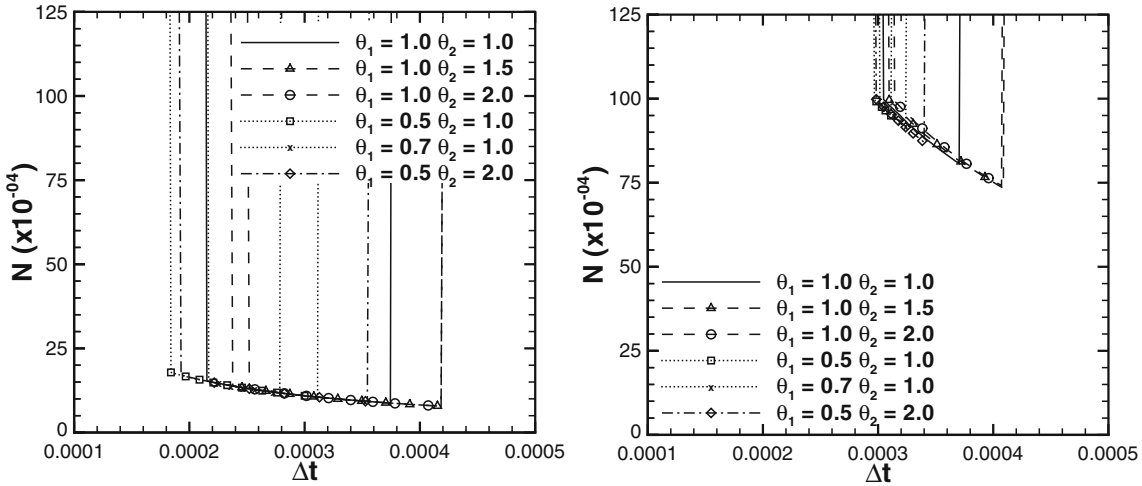

Fig. 6 Iterations required for convergence with MGM at $R = 5$ (*left*) and $R = 87$ (*right*)

Once the disturbance maximum amplitude became equal to 10% of the steady-state one, both SFD and MGM were turned on. However, it was not possible to recover $u(t \to \infty) \simeq u_s$ using SFD, which was actually not able to provide any damping whatsoever. This result is yet another evidence that SFD cannot damp stationary modes. The number of iterations N required by MGM to reach $|(u^{n+1} - u^n)/(u^2 - u^1)| = 10^{-8}$ is shown in Fig. 6 for both convectively (left) and absolutely (right) unstable conditions $R = 5$ and $R = 87$, respectively. As happened in the previous test case, there is a maximum Δt beyond which it is no longer possible to reach the required tolerance, which is imposed by nonlinear effects. On the other hand, this figure also shows a minimum Δt below which the same problem happens, but now it is caused by the linear numerical instability shown in Fig. 2 for positive but small λ. In this test case, however, the optimal scheme has $\theta_1 = 1$ and θ_2 between 1.5 and 2. Although IE reaches steady-state, it is not optimal since the maximum Δt imposed by nonlinear effects does not allow it to reach smaller gains.

3.3 Advection of entropy disturbances

The advection of marginally stable 1D entropy disturbances at a Mach number of $M = 10^{-3}$ is considered as the next test case. A low Mach preconditioned density-based method is applied to the compressible governing equations,

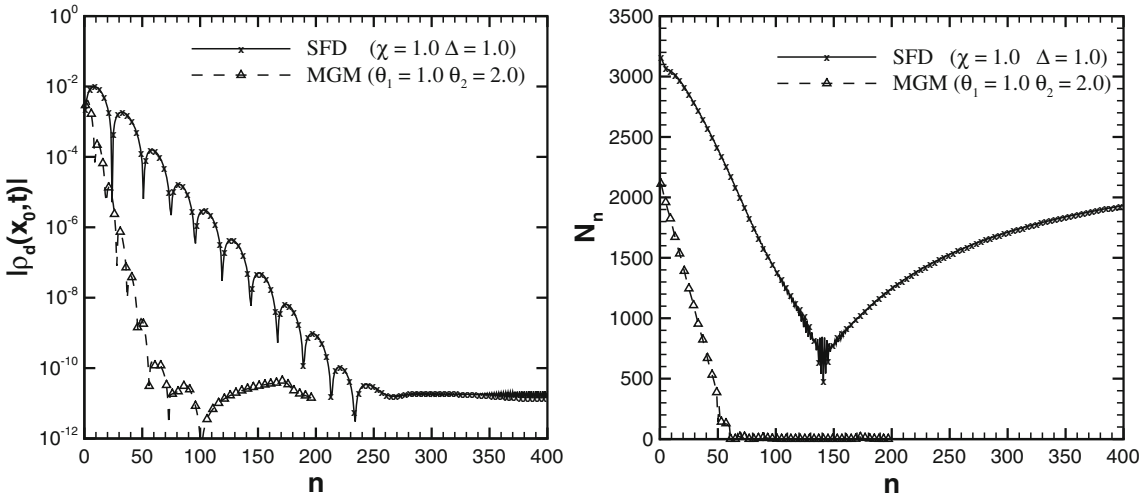

Fig. 7 Dimensionless disturbance measured at $x_0 = l_0/2$ (*left*) and pseudo-time iterations (*right*) per physical-time step for a single frequency perturbation

$$\mathbf{\Gamma}\frac{\partial \hat{\mathbf{q}}}{\partial \tau} = \mathbf{f}(\mathbf{q}) - \frac{\partial \mathbf{q}}{\partial t}, \tag{14}$$

in order to solve this problem, where $\mathbf{\Gamma}$ is the low Mach preconditioning matrix, $\hat{\mathbf{q}} = \{P_h, u, T\}$ is the primitive variable vector, $\mathbf{q} = \{\rho, \rho u, \rho E\}$ is the conservative variable vector, τ is the pseudo-time, t is the physical-time and $\mathbf{f}(\mathbf{q}) = 0$ represents the steady 1D Navier-Stokes equations. Specific details about any additional variables and simulation parameters not described here as well as code verification are discussed elsewhere [18]. In this study, the same tolerance prescribed as stopping criterium for the physical-time convergence toward steady-state, $|(\rho^{n+1} - \rho^n)/(\rho^2 - \rho^1)| = 10^{-6}$, was also used for the pseudo-time iterations during each physical-time step. Only optimal results from both MGM and SFD are shown from this point on.

First, a single disturbance with a domain size l_0 wavelength is introduced, leading to an unsteady flow characterized by a single frequency [18]. Figure 7 shows density disturbances (left) and number of pseudo-time iterations (right) per physical-time step that optimal MGM and SFD schemes take to reach steady-state. Although both reach steady-state at approximately the same physical-time t (not shown here), the number of physical-time steps n they require to do so is $n = 50$ and 213, respectively. This difference is shown on the left plot of this figure and occurs because both schemes use different Δt, 0.096 and 0.288 for SFD and MGM, respectively. SFD solves an additional differential equation that represents a filtering procedure originally defined as an integration. Since this integration must be accurately performed for the filter to work, its differential form must be accurately marched in time even though only the steady-state matters. This means SFD requires a relatively small Δt to work well. On the other hand, MGM can use as large a Δt as allowed by nonlinear effects and linear stability requirements. There is also a difference between the number of pseudo-time iterations N_n per n of MGM and SFD, as shown on the right plot of the same figure. N_n decreases to 1 at steady-state for MGM. This is due to the fact that N_n is controlled by the gain of the marching schemes employed in physical and pseudo-time, which never changes for a fixed time step. Hence, a solution obtained at n becomes an increasingly better initial guess for the pseudo-time iteration procedure that yields a solution at $n+1$ as steady-state is approached. The same is not true for SFD, since its N_n actually increases with n after an initial decrease. Although SFD uses the same marching scheme in pseudo-time as MGM, it uses CN2 in physical-time instead. It can afford to do so because its physical-time convergence is controlled by the source term added to the governing equations. However, this source term is zero at steady-state, which means its ability to maintain the unsteady solver at steady-state disappears. As the solver moves away from this limit though, the source term become nonzero again, driving the solver back to steady-state. These unsteady oscillations explain why the solution at n never becomes an ideal initial guess for the pseudo-time iteration that yields the solution at $n + 1$ with SFD. As a consequence, N_n never reaches 1 and the total iteration count $N = \sum N_n$ is also smaller in MGM than SFD when using these marching schemes with sub-iterations, approximately 5.2 times so in this test case.

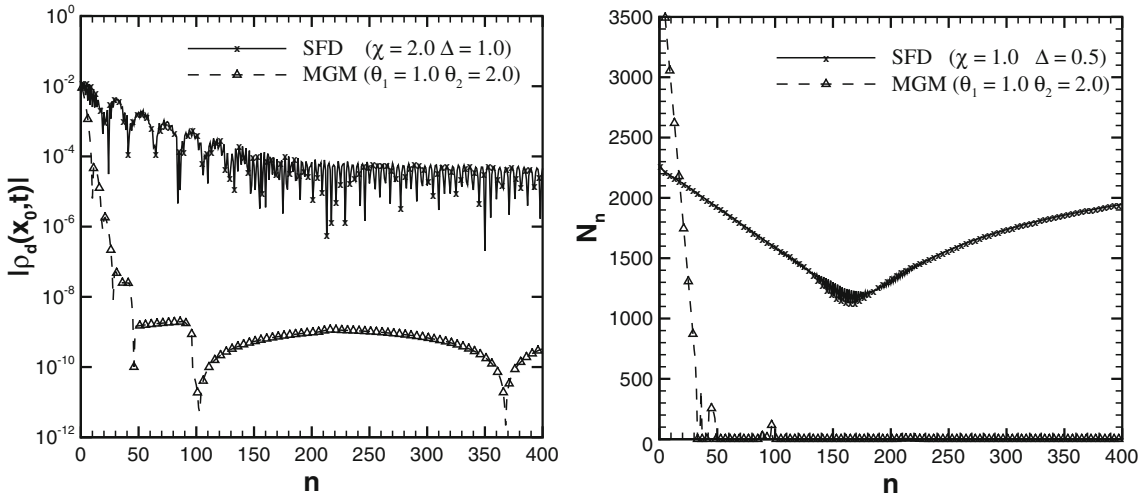

Fig. 8 Same as Fig. 7 but for multiple frequency perturbation

An additional simulation was considered for this particular test case, where the density initial condition takes the form of $\rho/\rho_0 = 1 + 2\,\delta_0\,\mathrm{IF}[\,x/l_0 < 1/2\,,\; x/l_0\,,\; x/l_0 - 1\,]$, where δ_0 is the initial disturbance amplitude. This leads to a marginally stable unsteady flow characterized by several frequencies. MGM and SFD are run in a similar way as done in the single frequency case and results are shown in Fig. 8. Despite qualitative similarities, a few important quantitative differences exist. An MGM scheme with $\theta_1 = 1$ and $\theta_2 = 2$ is still the optimal choice, but it requires approximately 24.5% more iterations to reach the same steady-state accuracy. This occurs at $n = 51$. SFD, on the other hand, appears not capable of generating a steady-state with the same tolerance. It takes SFD approximately 6.3 times more total iterations than MGM to reach $n = 273$, where the resulting disturbance amplitude is still 4 orders of magnitude higher than the imposed tolerance. Although one would have to employ multiple filters to improve the performance of SFD in this case (Schlatter, P. (2015), Personal communication), it is important to emphasize that MGM can be used when multiple frequencies are present without any modifications.

3.4 Planar mixing-layer

Absolutely unstable planar mixing-layers are simulated next as a final test. Simulations capture the linear and nonlinear growth of incompressible and inviscid disturbances with the 2D version of Eq. (14) solved with $M = 10^{-3}$, which were verified and validated elsewhere [3]. Once the most unstable linear mode introduced in the initial condition reached a 10% amplitude, i.e. before nonlinear effects can become significant, both steady-state generation methods were turned on. A relative physical-time tolerance was imposed on the stream wise velocity component using $|(u^{n+1} - u^n)/(u^2 - u^1)| = 10^{-6}$, where the same tolerance was employed in pseudo-time for each physical-time step. Only optimal results from MGM and SFD are shown.

Figure 9 shows stream wise velocity disturbances (left) and number of pseudo-time iterations (right) per physical-time step that optimal MGM and SFD schemes take to reach steady-state in a mixing layer with a velocity ratio of $VR = 1/2$. In this case, a relatively large time step Δt can be employed so the IE scheme is the optimal choice to reach steady-state among MGM schemes, which happens at $n = 34$. A slight oscillation exists around the steady-state after convergence, which is due to the linearly unstable nature of this flow. On the other hand, SFD fails to reach a steady-state with the same prescribed tolerance achieved by MGM. Furthermore, N_n once again does not reach 1 near steady-state, as observed in the previous subsection. It takes SFD approximately 27.6 times more iterations than MGM to reach $n = 557$, where a steady-state approximately 2 orders of magnitude less accurate than originally prescribed is achieved. N_n is also highly oscillatory for SFD, specially after $n > 50$. This is likely due to the linearly unstable nature of this flow. All remaining trends are qualitatively similar to what was observed in the previous test case, and no additional discussion is necessary here.

When the velocity ratio VR is decreased by 4 times, the most unstable linear mode growth rate doubles. Figure 10 shows the effects of this parametric change on the variables presented in Fig. 9. Once again, qualitative

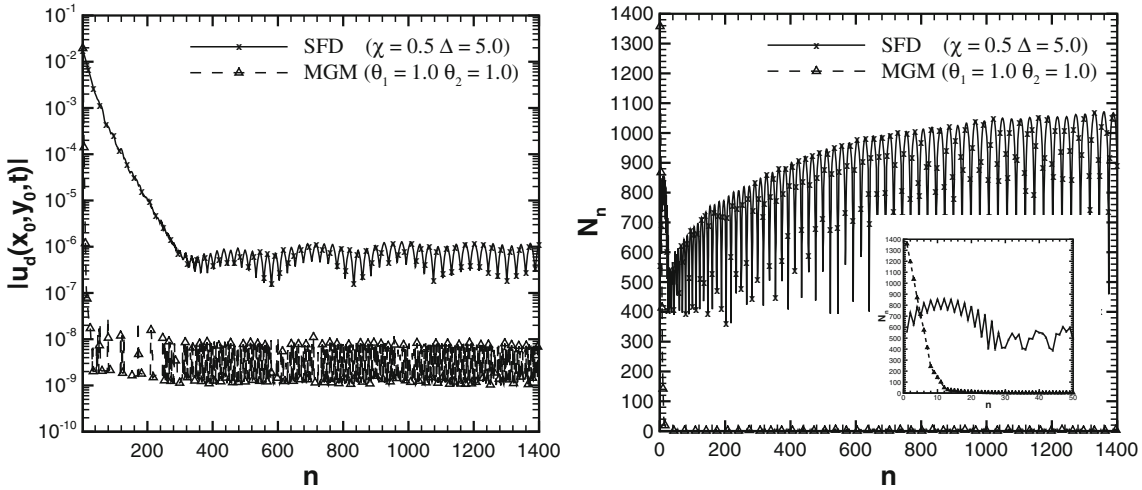

Fig. 9 Dimensionless disturbance measured at $x_0 = l_0/2$ and $y_0 = 0$ (*left*) and pseudo-time iterations (*right*) per physical-time step for velocity ratio $VR = 1/2$

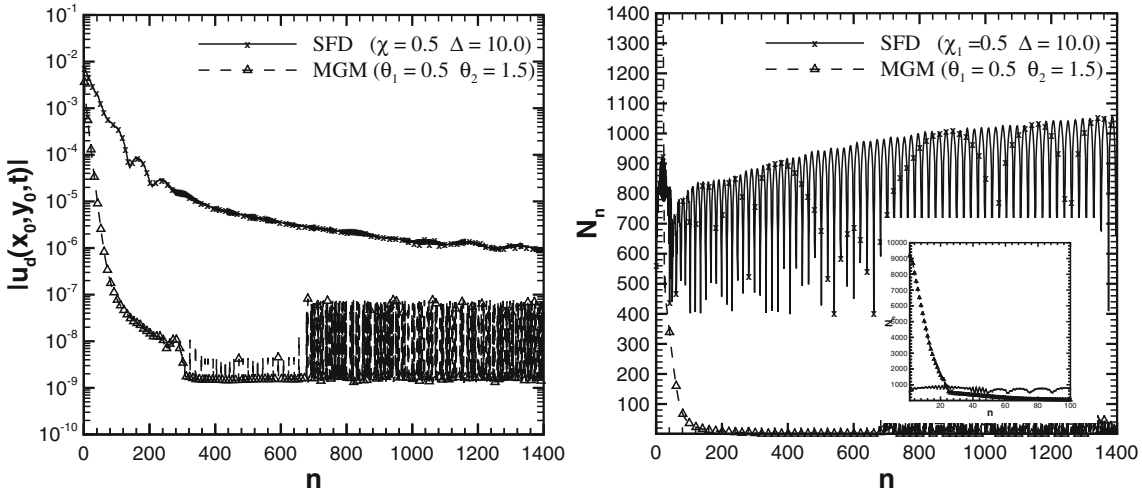

Fig. 10 Same as Fig. 9 but for velocity ratio $VR = 1/8$

trends are similar, but a few differences should be highlighted. IE is no longer numerically stable and a MGM scheme must be employed in its place to reach the required steady-state tolerances. This happens at $n = 309$ using $\theta_1 = 0.5$ and $\theta_2 = 1.5$, which represents the optimal choice. Its higher asymptotic gain combined with the stronger disturbance linear growth rates leads to slightly more than a 17 times increase in the total number of iterations N. Oscillations after convergence also increase in magnitude for the same reasons, getting strong enough to actually make $1 < N_n < 50$ for $n > 700$. SFD cannot convergence to a steady-state with the originally prescribed tolerance, but it does converge to one with approximately the same tolerance achieved with $VR = 1/2$. However, it does so using slightly different parameters and slightly more than 1.4 times its previous total number of iterations. Nevertheless, MGM still requires approximately 2.3 times less total iterations than SFD to reach a steady-state 2 orders of magnitude less accurate than the original tolerance.

In both temporally unstable and spatially periodic planar mixing-layer test cases, only a single disturbance was directly excited by the initial conditions. For this reason, one might be inclined to assume that the vanishing force term was responsible for the less accurate steady-states reached by SFD. However, the true cause of these inaccuracies is the presence of a broad range of unstable wave numbers, each one with its respective unstable frequency. Although they are not directly excited, round-off errors guarantee they are always indirectly excited in a simulation. The only difference between both cases is the excitation amplitude. Hence, the presence of multiple unstable frequencies is the real reason behind the SFD steady-state accuracy loss in these cases.

This issue is not uncommon in complex flows. In fact, similar steady-state errors have been observed in other studies (Schlatter, P. (2015), Personal communication). Nevertheless, it is important to note that the presence of multiple unstable frequencies in difference cases can be induced by different mechanisms, such as nonlinearities, transient growth, absolute instability with multiple pinching points, global instability with multiple self-selected frequencies, etc.

4 Conclusions

Steady-states have been traditionally obtained with Newton-type methods, but these methods are strongly dependent on accurate initial conditions for convergence and use steady codes that often require large computer resources. Selective frequency damping (SFD) has been proposed as an alternative 10 years ago. It has become popular because it can be easily implemented in an existing unsteady code and is rather insensitive to initial conditions.

However, the present paper has confirmed some limitations of SFD and found additional ones. They are itemized below:

- It generates schemes that are linearly stable but not consistent, since it alters the original unsteady problem by introducing a source term. This term is the driving force behind the ability of SFD to generate steady-states. On the other hand, it decreases in magnitude as the target steady-state is approached, actually disappearing at this limit. However, it cannot disappear entirely otherwise the steady-state cannot be maintained. The resulting weak unsteadiness leads to a couple of important issues. The first one is related to the higher computer cost of SFD. When used with marching schemes that require sub-iterations, the number of sub-iterations never decreases to one even after steady-state is supposedly reached. The second issue is related to the lower accuracy of SFD. It tends to leave a small error residue on the steady-state it finds. Furthermore, this error seems to increase in magnitude as the flow becomes more temporally unstable.
- It requires an accurate unsteady simulation even though only steady-states are pursued. This is due to the additional differential equation included by this method to replace a numerical integration, which must be accurately performed for the filtering procedure to work. Hence, it appears that SFD is more suitable to marching schemes with high accuracy-order and/or strong linear stability. The former leads to smaller errors at smaller time steps, whereas the latter leads to a decrease in error propagation. One more remark must be made here, which is also related to the previous limitation. Theoretically, one should be able to increase the time step as steady-state is approached in order to reduce computer cost. However, this seems to enhance the weak unsteadiness that remains near steady-state, making both issues related to it and discussed above quite worse. For this reason, such a procedure was not used in the present paper.
- It seems unable to generate a steady-state when the flow is unstable to stationary disturbances, whether this is instability is convective or absolute. Although it might be possible to use a zero frequency filter, no such filter has been developed yet as far as the authors are aware.
- It has difficulties generating accurate steady-states if multiple frequencies are present in a flow. This issue could probably be resolved by including additional filters, but no such attempt was made here.

Some researchers have also used an implicit Euler scheme to drive unsteady equations to steady-state, although to a much lesser extent. This scheme is usually chosen for this task since it is numerically L-stable for both physically stable and unstable linear systems. However, it does have a region of linear numerical instability associated with a weak physical instability. Hence, this scheme diverges when nonlinearities do not allow the use of large enough time steps to place all physically unstable eigenvalues outside of this numerically unstable region. In the present paper, a modification based on numerical consistency and linear stability reduces the size of this numerically unstable region, greatly extending the applicability of such schemes. This approach to deriving marching schemes for the generation of steady-states is called a minimal gain marching (MGM) methodology. The new set of implicit multi-step schemes obtained from this methodology is called MGM schemes. Their advantages over SFD are:

- They are linearly stable and consistent, which means the driving force behind the ability of MGM schemes to march toward steady-state comes from the built-in asymptotic properties of these marching schemes. One such property is the gain, since all available coefficients of the marching scheme were chosen to numerically stabilize as much as possible of the physically stable and unstable regions. The other property is the time step, which is then chosen in such a way as to place all stable and unstable spectra within this

numerically stabilized regions. Since the gain remains unaltered once the time step is fixed, the driving force is always the same. Hence, two important advantages appear. The first one is related to the lower cost of MGM. When used with marching schemes that require sub-iterations, the number of sub-iterations decreases to one once steady-state is reached. The second advantage is related to the higher accuracy of MGM. Steady-states are as accurate as allowed by the error tolerances imposed.
- Consistency requires first-order accuracy in time, although higher orders can be achieved. Furthermore, consistency guarantees that the temporal accuracy of the MGM scheme does not affect the spatial accuracy of the steady-state it generates. This means accurate unsteady simulations are not required and, hence, the time step can be chosen to yield the smallest gain, contributing to the lower cost of MGM.
- They are able to generate steady-states when the flow field is unstable to stationary as well as oscillatory disturbances, whether this instability is convective or absolute.
- The presence of multiple and distinct unstable frequencies does not affect in any significant way the ability of MGM schemes to generate steady-states.

Despite these advantages of MGM over SFD, one important disadvantage remains. SFD can be easily applied to explicit and implicit schemes as well as multi-step and multi-stage schemes. On the other hand, MGM has only been shown here to work with implicit multi-step schemes. It should be possible to adapt implicit multi-stage schemes to satisfy a MGM methodology, since one can already find in the literature versions of implicit Runge-Kutta schemes that are numerically stable when applied to physically stable and unstable linear problems. However, the same is not true for explicit schemes as far as the authors are aware. All numerical experiments attempted by the authors with the free coefficients in Eq. (7) for explicit multi-step schemes ($b_{+1} = 0$) were not able to numerically stabilize ($|G| < 1$) the physically unstable region ($\lambda > 0$) for any time step Δt. Similar experiments for explicit multi-stage schemes have not yet been performed, but are likely to yield similar results. Hence, short of directly coding an implicit marching scheme, the only consistent approach to enable the implementation of implicit MGM schemes on originally explicit marching schemes appears to be dual-time stepping (DTS). In this case, the original explicit scheme is moved to pseudo-time and the implicit MGM scheme is applied to physical-time. During each physical-time step, one must perform sub-iterations in order to reach pseudo-time steady-state. As a consequence, simulations with this MGM-DTS scheme should require more computer time than the ones with the implicit MGM scheme discussed in the present paper. Nevertheless, the former is much simpler to code than the latter and would not affect the parallelization efficiency of the original explicit scheme. However, it is difficult to know at this point if MGM-DTS would outperform SFD or not. There are clearly a lot of questions that still need to be answered with the MGM methodology. For these reasons, at the present time, the authors do recommend using SFD, when the following conditions are met:

- Only explicit marching schemes are available;
- Flow is unstable to a single nonzero frequency disturbance;

noting that both convergence and accuracy of SFD deteriorate when more than one unstable frequency exists. SFD performed best for the Lorenz problem, where only a single nonzero unstable frequency exists. In all other test cases, convergence and/or accuracy issues were observed.

Acknowledgements The authors would like to thank the financial support received from CNPq through Grant 481072/2012-8 and FAPERJ through Grant E-26/201.524/2014.

References

1. Åkervik, E., Brandt, L., Henningson, D.S., Hoepffner, J., Marxen, O., Schlatter, P.: Steady solutions of the Navier-Stokes equations by selective frequency damping. Phys. Fluids **18**(6), 068102 (2006)
2. Åkervik, E., Hœpffner, J., Ehrenstein, U., Henningson, D.S.: Optimal growth, model reduction and control in a separated boundary-layer flow using global eigenmodes. J. Fluid Mech. **579**, 305–314 (2007)
3. Alves, L.S.B.: Preconditioned implicit Runge–Kutta schemes for unsteady simulations of low mach number compressible flows. In: Idelsohn, S., Sonzogni, V., Coutinho, A., Cruchaga, M., Lew, A., Cerrolaza M. (eds.) 1st Pan-American Congress on Computational Mechanics (2015)
4. Alves, L.S.B., Kelly, R.E., Karagozian, A.R.: Transverse jet shear layer instabilities. Part II: linear analysis for large jet-to-crossflow velocity ratios. J. Fluid Mech. **602**, 383–401 (2008)
5. Bagheri, S., Schlatter, P., Schmid, P.J., Henningson, D.S.: Global stability of a jet in crossflow. J. Fluid Mech. **624**, 33–44 (2009)
6. Barletta, A., Alves, L.S.B.: Transition to absolute instability for (not so) dummies (2014). arXiv:1403.5794

7. Barone, M.F., Lele, S.K.: Receptivity of the compressible mixing layer. J. Fluid Mech. **540**, 301–335 (2005)
8. Bijl, H., Carpenter, M.H., Vatsa, V.N., Kennedy, C.A.: Implicit time integration schemes for the unsteady compressible Navier–Stokes equations: laminar flow. J. Comput. Phys. **179**, 313–329 (2002)
9. Blaschak, J.G., Kriegsmann, G.A.: A comparative study of absorbing boundary conditions. J. Comput. Phys. **77**, 109–139 (1988)
10. Bodony, D.J.: An analysis of sponge zones for computational fluid mechanics. J. Comput. Phys. **212**(2), 681–702 (2006)
11. Brevdo, L., Laure, P., Dias, F., Bridges, T.J.: Linear pulse structure and signalling in a film flow on an inclined plane. J. Fluid Mech. **396**, 37–71 (1999)
12. Chomaz, J.M.: Global instabilities in spatially developing flows: non-normality and nonlinearity. Annu. Rev. Fluid Mech. **37**, 357–392 (2005)
13. Collis, S.S., Lele, S.K.: Receptivity to surface roughness near a swept leading edge. J. Fluid Mech. **380**, 141–168 (1999)
14. Colonius, T.: Modelling artificial boundary conditions for compressible flow. Annu. Rev. Fluid Mech. **136**, 315–345 (2004)
15. Colonius, T., Lele, S.K.: Computational aeroacoustics: progress on nonlinear problems of sound generation. Prog. Aerosp. Sci. **40**, 345–416 (2004)
16. Cunha, G., Passaggia, P.Y., Lazareff, M.: Optimization of the selective frequency damping parameters using model reduction. Phys. Fluids **27**(094103), 1–22 (2015)
17. Dahlquist, G.: A special stability problem for linear multistep methods. BIT Numer. Math. **3**, 27–43 (1963)
18. Falcao, C.E.G., Medeiros, F.E.L., Alves, L.S.B.: Implicit Runge–Kutta physical-time marching in low mach preconditioned density-based methods. In: 7th AIAA Theoretical Fluid Mechanics Conference, AIAA 2014-3085. AIAA Aviation (2014)
19. Germanos, R.A.C., de Souza, L.F., de Medeiros, M.A.F.: Numerical investigation of the three-dimensional secondary instabilities in the time-developing compressible mixing layer. J. Braz. Soc. Mech. Sci. Eng. **31**(2), 125–136 (2009)
20. Jones, L.E., Sandberg, R.D., Sandham, N.D.: Stability and receptivity characteristics of a laminar separation bubble on an aerofoil. J. Fluid Mech. **648**, 257–296 (2010)
21. Jordi, B.E., Cotter, C.J., Sherwin, S.J.: Encapsulated formulation of the selective frequency damping method. Phys. Fluids **26**(034101), 1–10 (2014)
22. Jordi, B.E., Cotter, C.J., Sherwin, S.J.: An adaptive selective frequency damping method. Phys. Fluids **27**(094104), 1–8 (2015)
23. Kelly, R.E., Alves, L.S.B.: A uniformly valid asymptotic solution for the transverse jet and its linear stability analysis. Philos. Trans. R. Soc. Lond. Ser. A Math. Phys. Sci. **366**, 2729–2744 (2008)
24. Knoll, D.A., Keyes, D.E.: Jacobian-free Newton–Krylov method: a survey of approaches and applications. J. Comput. Phys. **193**, 357–397 (2004)
25. Lardjane, N., Fedioun, I., Gokalp, I.: Accurate initial conditions for the direct numerical simulation of temporal compressible binary shear layers with high density ratio. Comput. Fluids **33**, 549–576 (2004)
26. Lax, P.D., Richtmyer, R.D.: Survey of the stability of linear finite difference equations. Commun. Pure Appl. Math. **IX**, 267–293 (1956)
27. Loiseau, J.C., Robinet, J.C., Cherubini, S., Leriche, E.: Investigation of the roughness-induced transition: global stability analyses and direct numerical simulations. J. Fluid Mech. **760**, 175–211 (2014)
28. Lomax, H., Pulliam, T.H., Zingg, D.W.: Fundamentals of Computational Fluid Dynamics. Scientific Computation. Springer, Berlin (2001)
29. Megerian, S., Davitian, J., Alves, L.S.B., Karagozian, A.R.: Transverse jet shear layer instabilities. Part I: experimental studies. J. Fluid Mech. **593**, 93–129 (2007)
30. Michalke, A.: Survey on jet instability theory. Prog. Aerosp. Sci. **21**, 159–199 (1984)
31. Pier, B.: Local and global instabilities in the wake of a sphere. J. Fluid Mech. **603**, 39–61 (2008)
32. Pulliam, T.H., Steger, J.L.: Implicit finite-difference simulations of three-dimensional compressible flow. AIAA J. **18**(2), 159–167 (1980)
33. Saric, W.S., Reed, H.L., White, E.B.: Stability and transition of three-dimensional boundary-layers. Annu. Rev. Fluid Dyn. **35**, 413–440 (2003)
34. Schmid, P.J.: Nonmodal stability theory. Annu. Rev. Fluid Mech. **39**, 129–162 (2007)
35. Sparrow, C.: The Lorenz Equations: Bifurcations, Chaos and Strange Attractors, Applied Mathematical Sciences, vol. 41. Springer, New York (1982)
36. Steinberg, S., Roache, P.J.: Symbolic manipulation and computational fluid dynamics. J. Comput. Phys. **57**, 251–284 (1985)
37. Teixeira, R.S., Alves, L.S.B.: Modeling far field entrainment in compressible flows. Int. J. Comput. Fluid Dyn. **26**, 67–78 (2012)
38. Theofilis, V.: Global linear instability. Annu. Rev. Fluid Mech. **43**, 319–352 (2011)
39. Wang, L., Mavriplis, D.J.: Implicit solution of the unsteady Euler equations for high-order accurate discontinuous Galerkin discretizations. J. Comput. Phys. **225**(2), 1994–2015 (2007)